Experimental Investigation of the Wind Loading on Solar Panels: Effects of Clearance off Flat Roofs

Hatem Alrawashdeh, A.M.ASCE[1]; and Ted Stathopoulos, F.ASCE[2]

Abstract: The paper presents the results of a comprehensive wind tunnel study dedicated to addressing the effects of the underneath array clearance on wind loading of roof-mounted solar panels. Indeed, the array clearance has a crucial influence in many respects ranging from its consideration in the wind tunnel modeling to its impact on structural safety. A set of atmospheric wind tunnel experiments was carried out on three configurations of a multipanel solar array mounted on a flat roof immersed in a simulated atmospheric flow of open-country exposure. The solar array was placed at three clearance heights above the roof, namely, 0, 20, and 40 cm (in full scale). Wind tunnel measurements of the mean and peak pressures on both bottom and top surfaces of the solar panels as well as of net pressures across the panels were carried out. The results show that the impact of the underneath array clearance on the panel wind-induced pressures depends highly on the wind direction and the location of the panel within the array. Generally, the wind-induced pressures on solar panels when lowering the array clearance become quite severe and may peel off the panels from the supporting racking system; on the other hand, at such clearance installation, the panels are subjected to lower downward net pressure. Furthermore, the study highlights the potential uncertainties in the wind tunnel experimental results that could be deemed as actual design loadings when the underneath clearance is of concern. This has important ramifications on the formulation of design provisions to be used by solar panel professionals. **DOI: 10.1061/JSENDH/STENG-10957.** © *2022 American Society of Civil Engineers.*

Author keywords: Codes and standards; Air clearance; Solar panels; Wind pressures; Wind tunnel.

Introduction

Renewable energy projects have become very popular worldwide in recent decades in response to the calls for a sustainable future. Solar technology and energy have significant contributions to achieving sustainable energy development of safe, clean, and constantly replenished resources. Utility-scale solar photovoltaic (PV) projects, along with commercial and residential installations, experience rapid growth. Clearly, efforts to promote such installations encompass the safety and operation of their structures against several environmental impacts, primarily wind-induced pressures.

Since the turn of the century, a growing number of studies have been undertaken to identify and assess the impact of geometric parameters on wind-induced pressures on roof-mounted solar panels, including building shape and size, panel location on the roof, panel size, panel tilt, interpanel spacing, and wind deflectors. However, several research questions about issues such as the effect of the underneath array air gap on the wind loading on the panels have not yet been answered. This air gap, also referred to as underneath array clearance off the roof, is necessary for natural cooling by convection on the bottom surface of PV modules to maintain better electrical generation efficiency. Thus, mounting the solar array at a higher clearance off the roof is a legitimate requirement to increase the ventilation, and hence to improve the fire resistance of the PV modules and the roof. Furthermore, installing the solar array at higher clearance may have advantages in regions exposed to high snow, notably by placing the array further from the snow built up on the roof and by providing more flexibility for cleaning the snow accumulated on the roof. Changing the array clearance may, however, result in disturbing the wind loadings induced on the PV modules or the racking system.

In the literature, some studies of wind loadings on solar panels tended to disregard the array clearance in their wind tunnel modeling due to the limitations on the wind tunnel model scale, either by placing the solar array directly on the roof or, indiscriminately, at a certain possible clearance above the roof just to consider the airflow underneath the array. On the other hand, some studies have dealt with the array clearance of solar panels mounted parallel to sloped roofs or tilted on flat roofs. As indicated in Table 1, which provides a summary of the geometric parameters of these studies, most focused on solar panels mounted on sloped roofs (Stenabaugh et al. 2010, 2015; Ginger et al. 2011; Geurts and Blackmore 2013; Leitch et al. 2016; Naeiji et al. 2017), because particularly for such installation the array clearance plays a significant role in the equalization of the pressures induced on the panel surfaces.

In comparison, limited studies have touched on the influence of the array clearance on wind loading of solar panels tilted on flat roofs. Kopp (2014) examined experimentally the effect of the clearance on the extreme area-averaged force coefficients, i.e., the most critical coefficient values enveloped from all wind directions. In this investigation, the solar array was placed at three heights above the roof (9, 41, and 102 cm, in full scale) at two tilt angles 5° and 20°. It was found that the array clearance has a minimum impact on the pressure envelope curves for the configurations considered, except for the largest clearance (102 cm) and the lowest tilt (5°), at which a considerable increase in the envelope curves of the negative area-averaged force coefficients was observed in the range of 1.3 to 1.6. Naeiji et al. (2017) examined the extreme force

[1]Ph.D. Candidate, Dept. of Building, Civil and Environmental Engineering, Concordia Univ., Montreal, QC, Canada (corresponding author). ORCID: https://orcid.org/0000-0002-9802-3213. Email: h_alraw@encs.concordia.ca

[2]Professor, Dept. of Building, Civil and Environmental Engineering, Concordia Univ., Montreal, QC, Canada. Email: statho@bcee.concordia.ca

Note. This manuscript was submitted on September 30, 2021; approved on August 8, 2022No Epub Date. Discussion period open until 0, 0; separate discussions must be submitted for individual papers. This paper is part of the ***Journal of Structural Engineering***, © ASCE, ISSN 0733-9445.

PROOF ONLY

Table 1. Studies touching on the clearance effect

Installation	Reference	Exposure	Scale	Min Rex10^5	Building geometry: Height, H	Length, L	Width, W	Roof slope, θ_B	Panel geometry: Chord length, L_P	Width, W_P	Tilt, θ	Underneath clearance, G
Flushed on sloped roof	Stenabaugh et al. (2010)	Open $z_o = 0.01$ m	1:20	3.3	7.8	15.0	10.0	30.0	1.5	0.5	30	0.04
					8.4		12.3	45.0			45	0.08
	Ginger et al. (2011)	Open	1:20	—	3.0	21.0	10.0	7.5	1.7	1.0	7.5	0.10
					3.4			15.0	3.4		15.0	0.20
					3.7			22.5			22.5	
	Geurts and Blackmore (2013)	Open $z_o = 0.03$ m	1:100	—	8.6	—	—	42.0	1.5	1.0	—	0.03
												0.05
												0.10
												0.20
	Stenabaugh et al. (2015)	Open $z_o = 0.01$ m	1:20	3.0	6.0	15.0	12.3	30.0	1.5	0.5	30	0.00
							7.5					0.02
												0.04
												0.08
												0.14
												0.20
	Leitch et al. (2016)	Suburban	1:20	—	2.7	21.0	10.0	7.5	7.0	1.7	7.5	0.10
								15.0			15.0	0.20
								22.5			22.5	
	Naeiji et al. (2017)	Suburban $\alpha = 0.18$ $z_o = 0.20$	1:6 (WoW)	0.83	6.5	13.7	9.1	Gable 14.0	2.0	1.0	14.0	0.30
					10.6			Hip 14.0				0.45
Tilted on flat roof	Kopp (2014)	Open $z_o = 0.03$ m	1:30	1.9	7.3	27.1	22.5	0	1.0	20	5	0.09
											20	0.41
												1.02
	Naeiji et al. (2017)	Suburban $\alpha = 0.18$ $z_o = 0.20$ m	1:6 (WoW)	0.83	6.6	13.7	9.1	0	2.0	1.0	20	0.30
					10.6						30	0.45
											40	
	Wang et al. (2020b)	Open $\alpha = 0.01$ m	1:50 (CFD)	—	20	26.0	26.3	0	2.0	21.0	15	0.30
												0.60

Note: All dimensions are in full scale, in meters and degrees.

coefficients averaged over the module area for array at two heights above the roof, namely, 30 and 45 cm, by using large-scale models (1:6) and found that the results show minor differences with the array air clearance.

A recent computational study using large eddy simulation (LES) by Wang et al. (2020b) also dealt with the array clearance effect. The study focused on the variation of the surface pressure coefficients at oblique wind directions, including 45° and 135°, at three different clearances above the roof (0, 30, and 60 cm). It was found that the gap size has a slight impact on the mean pressure coefficients on the top surface of the solar panels but a significant impact on the respective values induced on the bottom surface. In particular, the local suction on the bottom surface of the windward corner modules increases by a factor up to 2.0 in the presence of clearance.

Clearly, the previous studies of solar panels placed tilted on flat roofs provided only circumstantial and contradictory evidence for the importance of underneath array clearance effects. Indeed, the impact of the clearance on the wind loads on solar panels mounted tilted on flat roofs has not yet been comprehensively studied and the aerodynamic potential consequences of the array clearance have not been well understood. In addition, the current national wind codes and standards commonly used in professional practice, such as the North American wind codes and standards (NRCC 2015; SEAOC 2017; ASCE 2022) and the Japanese industrial standard (Japanese Standards Association 2017), do not address the impact of array clearance on wind loading.

Therefore, the question of the array clearance implications on wind loading of tilted solar panels on flat roofs became the incentive for conducting the present experimental study with the objective to thoroughly examine the dependence of wind-induced pressure on the underneath array clearance from aerodynamic and design perspectives. Furthermore, the current research strategy seeks to investigate how critical it is to preserve the solar panel clearance against any blockage introduced during the solar panel modeling in the wind tunnel by pressure taps tubing, depending on the details of the experimental methodology.

Methodology

Three sets of experiments were conducted in the atmospheric boundary layer wind tunnel of Concordia University. The blow-down tunnel is of the open-circuit type with a working section 1.80 m in width and 12.2 m in length, and has adjustable roof height in the range of 1.40 to 1.80 m. The tunnel is fitted with a turntable of 1.60-m diameter to enable the examination of different wind directions. This wind tunnel has been used for many codification-oriented studies, such as Stathopoulos and Dumitrescu-Brulotte (1989), Stathopoulos and Mohammadian (1991), Saathoff and Stathopoulos (1992), Stathopoulos et al. (2000, 2013), Candelario et al. (2014), and Alrawashdeh and Stathopoulos (2015). A detailed description of Concordia's boundary layer wind tunnel facility with its simulation characteristics is provided by Stathopoulos (1984).

PROOF ONLY

This section includes a description of boundary flow simulation, test model, and instrumentations and equipment that served to develop the experimental work of the present study.

Atmospheric Boundary Layer Simulation

The boundary layer flow of the wind tunnel is mainly developed using triangular boards, a steel plate, and carpet roughness. Four boards of the same triangular shape (spires), each of base width and height of 19 and 120 cm, respectively, were tied up side by side with a center-to-center distance of 36.5 cm to the screen of the tunnel entrance. The two end spires were positioned approximately 35 cm from tunnel sidewalls.

For the present study, all experiments were carried out in a fully developed flow over a simulated open-country exposure. The thick carpet furnished along the floor generates the intended velocity and turbulence profiles of a standard open-country exposure. Fig. 1(a) shows the variation of mean streamwise wind velocity ($\bar{U}$) and longitudinal turbulence intensity (I_u) with the height above the tunnel floor (Z) in the test section at the place of the model measured using a four-hole Cobra probe (TFI). In this figure, Z_g and $\bar{U}_g$ refer to the gradient height and the corresponding wind speed, respectively. The gradient wind speed ($\bar{U}_g$) was set at about 12.6 m/s at a velocity scale of 1:3 to duplicate the full-scale gradient velocity of 37.8 m/s. As set out in Fig. 1(a), the profile of the measured mean wind speed is best fitted by the logarithmic law model with a roughness length (z_o) of 0.01 cm on the wind tunnel scale and by the power-law with exponent $\alpha = 0.15$. Also, the vertical distribution of the turbulence intensity is fitted with a logarithmic function of the form $I_u = 0.9/\ln(Z/z_o)$, which is consistent with the approximate definition of the longitudinal turbulence intensity profile $I_u = 1.0/\ln(Z/z_o)$ specified by ASCE/SEI 49 (ASCE 2021).

The streamwise component of the turbulence integral length scale of the approach flow ($L_{u,x}$) is empirically determined at the height of $Z = 15.0$ cm above the wind tunnel floor using Cook's (1978) model

$$L_{u,x} = 25 \times (Z - d)^{0.35} \times z_o^{-0.063} \quad (1)$$

in which d = displacement height ($d = 0$ for open-country profile). For a scale factor of 1:500, $L_{u,x}$ is found to be 0.27 m on the wind tunnel scale.

Fig. 1(b) compares the spectrum of the streamwise wind tunnel flow measured using the four-hole Cobra probe (TFI) at the proposed height of the test model (i.e., $Z = 15.0$ cm above the wind tunnel floor) with the corresponding power spectrum model of von Kármán (1948) and Davenport (1961). It is also pertinent to point out that the full-scale von Kármán spectrum shown is interpolated for an integral scale of $L_{u,x} = 135$ m. Accordingly, the approach flow scale is 1:500, in which the gradient height of 60 cm developed above the wind tunnel floor is approximately equivalent to 300-m boundary layer thickness in full scale. Although the reduced power spectra are somewhat higher than the von Kármán and the Davenport spectra toward the end of the dissipation range, i.e., at higher reduced frequencies, the overall error introduced is rather small. Apparently, there are discrepancies about the various proposed spectra as well.

One primary research dilemma with testing solar panels in atmospheric boundary layer wind tunnel at a full-depth flow of open-country exposure is the geometric scaling of the test model. Most of the atmospheric boundary layer wind tunnels are developed for testing models of buildings at geometric test scaling in the range of 1:300 to 1:500. However, in the particular case of solar panels, the prototype size is a major constraint for proper geometric test scaling satisfying the similarity parameters between the approaching flow and the test models. Certainly, prototypes scaled down within this ratio will yield an untestable model of very small size. For instance, the most common size of individual solar PV cells, in this paper referred to as a module, used for commercial installation is 200 cm (chord length) by 100 cm (width) and at 1:500 scale its size will be experimentally untestable (i.e., 4.0 by 2.0 mm). Furthermore, considering such a modeling scale will result in distorting some layout features such as the air clearance between the roof and the solar array.

Several experimental and computational studies were primarily derived by the impetus of the geometric test scaling issue of different solar panel systems, namely, Aly and Bitsuamlak (2013) and Aly (2016) for a single solar panel mounted on the ground and

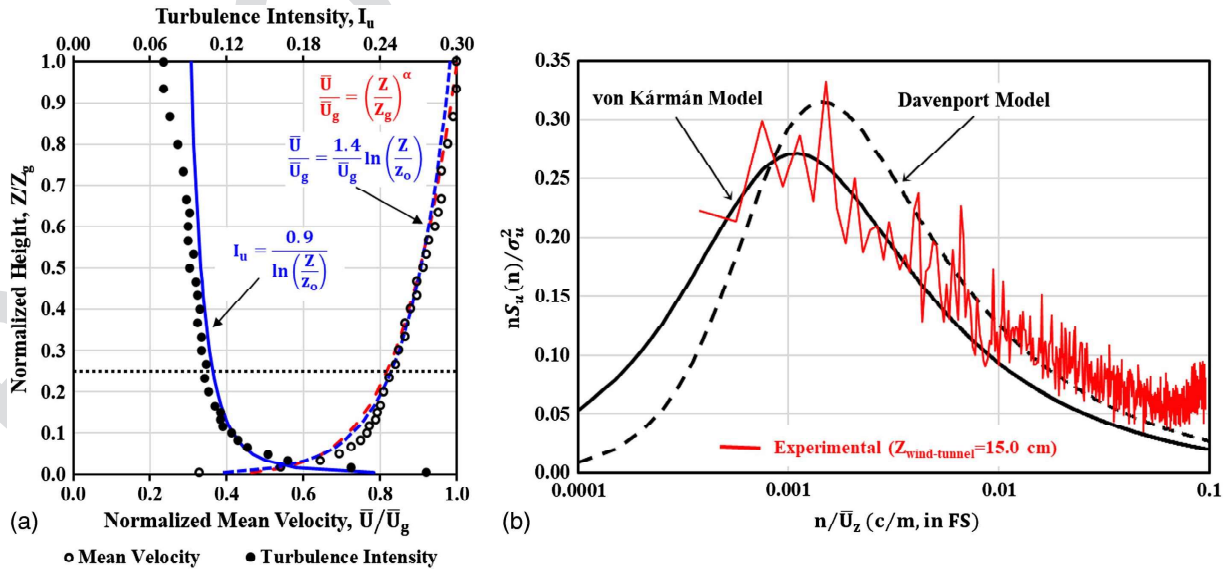

F1:1 F1:2 **Fig. 1.** Characteristics of the simulated wind tunnel flow: (a) profiles of streamwise mean wind speed and turbulence intensity; and (b) dimensionless spectrum of the streamwise velocity fluctuations.

PROOF ONLY

Alrawashdeh and Stathopoulos (2020) for solar panels mounted on flat roofs. Although the aforementioned studies have demonstrated that violating the geometric test scale yields discrepancies in the mean and peak force coefficients, the rightful size of the wind tunnel models for such structures is an actual impediment to upholding the flow simulation requirements.

Model Design and Arrangement

The selection of the building and the solar array configuration for the present study was guided by the fact that the building plane size has a significant impact on the solar panel wind loading (Kopp et al. 2012; Kopp 2014; Stathopoulos et al. 2014) and a larger number of panels would lead to better capturing the complexity of the wind interaction with the solar panels; hence, more aerodynamic events are promoted. It is also necessary to maintain a minimum wind tunnel blockage, which shall be less than the 5.0% limit specified by ASCE/SEI 49 (ASCE 2021).

All things considered, a building model with a flat roof of dimensions 28.0 and 54.0 cm and a height of 15.0 cm was devised for the current study. In line with the recommendation of ASCE/SEI 49 (ASCE 2021) for wind tunnel testing of rooftop solar panels, the considered solar array comprised eight panels (rows). The solar array was placed at a clearance height (G) of 0.8 cm above the roof at a tilt angle of 15°. The solar panel had a chord and span length of 4.0 and 20.0 cm, respectively. The array tilt angle was selected to reflect the content of the current wind codes and standards as viewed by the authors as critical tilt within the range of 5° and 20°. For instance, the National Building Code of Canada (NRCC 2015), SEAOC PV2 (SEAOC 2017), and ASCE/SEI 7 (ASCE 2022) prescribe the same design pressure coefficients for all installations with a tilt angle ranging from 0° and 15°; also, JIS C 8955 (Japanese Standards Association 2017) treats all installations of tilt between 10° and 50° similarly in terms of design pressure coefficients. Fig. 2 presents the test model installed on the turntable of the wind tunnel test section. The maximum blockage ratio of the test model is approximately 3.6% at the oblique wind direction and the minimum Reynolds number based on the model height is 10.5×10^4, which is approximately more than nine times larger than the minimum limit specified by ASCE/SEI 49 (ASCE 2021).

As mentioned previously, the common panel cord length is 200 cm (in full scale). Accordingly, the size of the wind tunnel model to the prototype is 1:50. In fact, such geometric test scaling has been used widely in the literature studies, including Cao et al. (2013) and Wang et al. (2018), or larger such as those mentioned in Table 1, without, however, examining the effect of this scale distortion on the measurement results. Fig. 3 shows the full-scale layout of the solar array and the building on which it is mounted.

Although there is no standard regulation on the size of the air clearance above the roof for solar panels tilted on flat roofs, Alberta Roofing Contractors Association (ARCA) standards (Alberta Infrastructure 2017) require the solar panels to be installed at a minimum clearance of 30.0 cm above the roof for construction warranty eligibility considerations. During the initial experimental setup, the clearance underneath the solar array was preserved at the typical height (i.e., $G = 40.0$ cm in full scale). Experimentally, to examine the impact of the solar array clearance off the roof during the modeling in the wind tunnel and carry out a parametric study, the solar array was placed at two additional clearance heights, including $G = 20$ cm and $G = 0$ cm, which respectively represent half of the typical clearance and no clearance. Indeed, the no clearance case ($G = 0$) could be viewed as a practical situation when the solar panels are exposed to heavy snow that may accumulate around the array.

The model of the solar panel was made of thin sandwiched metallic plates a total of 2.3 mm thick with identical pressure taps on both surfaces (top and bottom) to determine the pressure across the panel (net pressure). Each surface of the panel was equipped with three lines of pressure taps, in the middle and close to the edges for a total of 60 taps per panel, as illustrated in Fig. 3. The surface

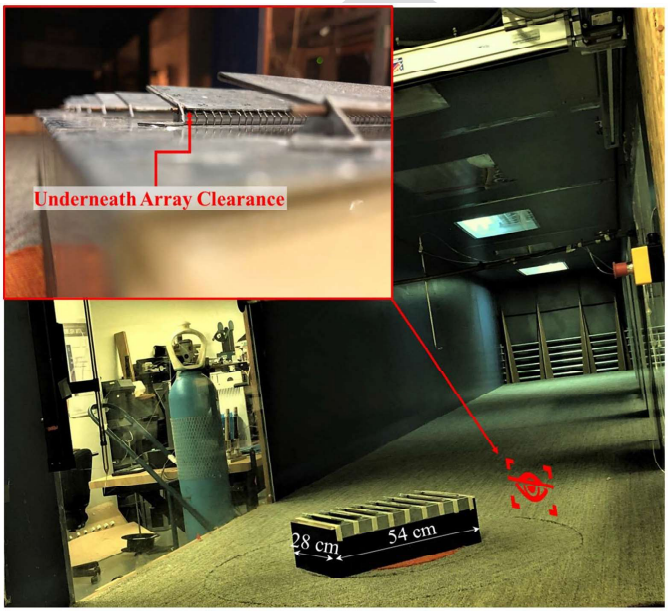

Fig. 2. Test model in the wind tunnel of Concordia University (panels are placed at typical clearance above the roof, $G = 40$ cm in full scale).

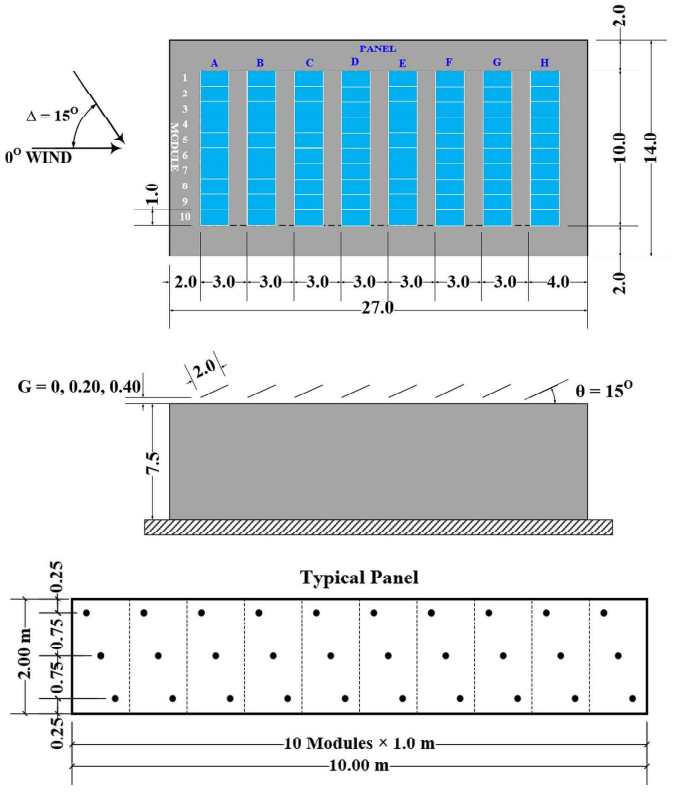

Fig. 3. Full-scale equivalent geometric details of the test model and typical solar panel surface with pressure taps (dimensions in meters).

PROOF COPY

pressure taps were connected to the channels of the urethane tubing of 550-mm length. Traditional custom-made brass restrictors were placed within the urethane tubes at a specific location (300 mm from the model pressure tap) to add damping to minimize the gain and phase shifts of pressure signals due to Helmholtz's resonance effects.

The pressure measurements were carried out by connecting the pressure taps to a Scanivalve system of miniature pressure scanners made up of an electronic pressure scanning module (model ZOC33) (each accepts up to 64 pneumatic inputs) and a digital service module (DSM 3400). The pressure scanners were calibrated to scan the pressure signals at a frequency of 300 Hz for a total period of 27 s on the wind tunnel model scale. In considering the similarity of geometric (H), time (T), and velocity ($\bar{U}$) scales in the wind tunnel with atmospheric conditions, expressed by Eq. (2), the time scale of the pressure measurements time series was found to be 1:16.7. Accordingly, the 27 s of the pressure time series are equivalent to 450 s in full scale. However, necessary adjustments were made to reference the pressure to 1,800-s dynamic velocity pressure using the well-known Durst curve (Durst 1960)

$$\frac{T_M}{T_F} = \frac{\bar{U}_F}{\bar{U}_M} \times \frac{H_M}{H_F} \tag{2}$$

in which F and M = full scale and model, respectively.

Analysis of Experimental Data

The instantaneous wind pressures over the solar panel surfaces at the measurement pressure taps were measured in the wind tunnel for all considered wind directions in terms of time history wind load. The wind directions considered in this study (0° to 180°) at increments of 15° are defined in Fig. 3, which shows that the wind direction at 0° angle corresponds to wind straight into the building edge. The measured pressures were normalized by the mean dynamic pressure measured at reference height to present them in the form of nondimensional pressure coefficients

$$C_p(t) = \frac{P_{\text{measured}}(t)}{\bar{q}_H}, \qquad \bar{q}_H = \frac{1}{2}\rho \bar{U}_H^2 \tag{3}$$

where C_p = instantaneous wind pressure coefficient of a particular measurement tap either on the top or bottom surface; P_{measured} = measured wind pressure at the pressure tap; $\bar{q}_H$ = mean value of the dynamic velocity pressure at roof height (H); ρ = density of the air; and $\bar{U}_H$ = mean value of the wind velocity at roof height.

The instantaneous local net pressure coefficient (referred to as force coefficient) is provided as the pressure difference between the top and bottom surfaces at a particular location, as follows:

$$C_F(t) = C_{P,\text{Top}}(t) - C_{P,\text{Bottom}}(t) \tag{4}$$

where $C_{p,\text{Top}}(t)$ and $C_{p,\text{Bottom}}(t)$ = instantaneous wind pressure coefficients of the counterpart measurement taps on top and bottom surfaces at a particular location on the panel, respectively. The top and bottom surfaces of the panel are the surfaces facing the sky and the building roof, respectively.

In addition to the local pressure and force coefficients obtained respectively by Eqs. (3) and (4), force coefficients versus the effective wind area of the panel, called the area-averaged force coefficients, are also the focus of the present study's attention. The instantaneous area-averaged force coefficients over effective panel area (A) were calculated for each wind direction by simultaneously integrating the local wind force coefficients after being factored by the contributing area to each location being considered in the effective area as follows:

$$C_{F,A}(t) = \frac{1}{\sum_{i=1}^{N} A_i} \sum_{i=1}^{N} C_{Fi}(t) \times A_i \tag{5}$$

where $C_{F,A}(t)$ = area-averaged wind force coefficients at an instant (t); A_i = contributing area to the ith local force coefficient; and N = number of local force coefficients in the specified area ($A = \sum_{i=1}^{N} A_i$). The area-averaged force coefficient was determined for various effective areas (A) ranging from 2.0 m^2 (area of one module) to 20.0 m^2 (area of entire panel) with an increment of a module area (2.0 m^2). For each effective area, the force coefficient was calculated at every possible existence on the panel. By way of illustration, Fig. 4 shows the possible effective wind areas of force coefficients that correspond to an area of three modules ($A = 6.0$ m^2). As can be seen, there are eight possible effective wind areas within the panel area for the force coefficients. The same operation was applied to calculate the force coefficients at effective wind areas ranging between 2.0 and 20.0 m^2 (e.g., nine possible areas were considered to determine the force coefficient of effective wind area $A = 4.0$ m^2). In the ultimate analysis, 55 effective areas were considered for the calculation of the area-averaged force coefficients for each panel at each wind direction. When the effective wind area (A) is equal to the area of a module or a panel, the area-averaged force coefficient is referred to as module force coefficient and panel force coefficient, respectively.

Fig. 5 depicts the sign convention adopted for the key measurement results provided in this paper. Accordingly, the surface mean and peak pressure coefficients (C_P and GC_P) are positive when the

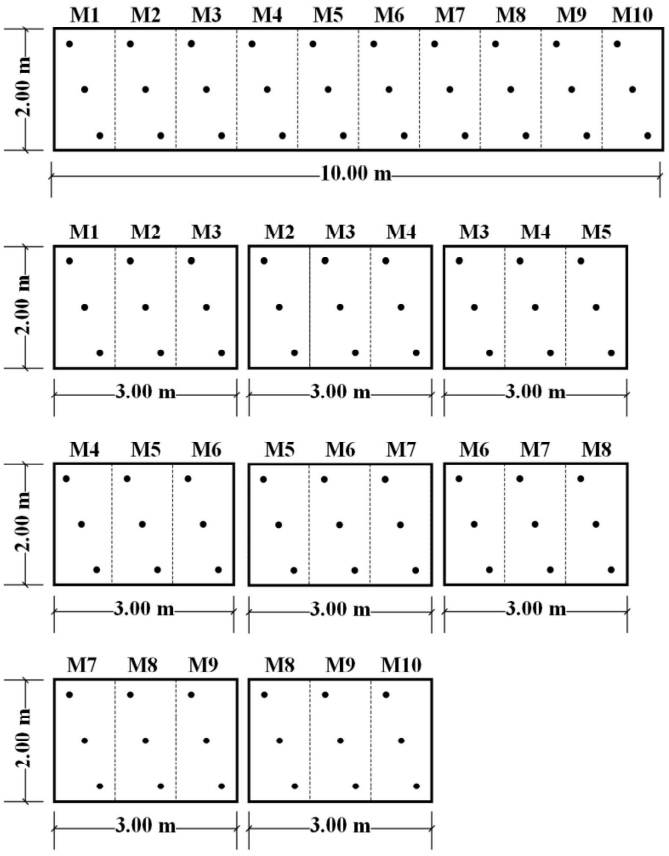

Fig. 4. Possible effective areas for C_F and GC_F corresponding to 6.0 m^2.

PROOF COPY

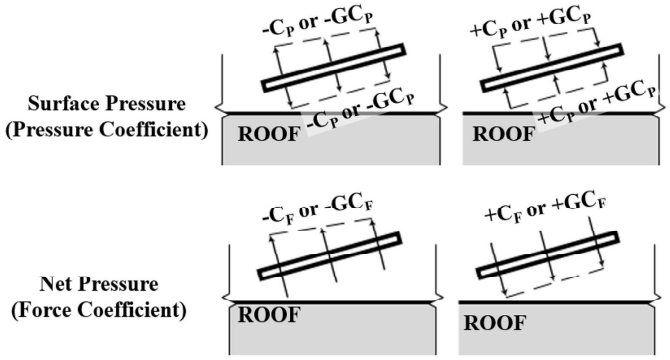

F5:1 F5:2 **Fig. 5.** Sign conventions for the pressure coefficients and force coefficients.

pressure acts toward the surface, and negative when the pressure acts away from the surface (suction). Also, the local and the area-averaged mean and peak force coefficients (C_F and GC_F) are negative if the pressure tends to peel off the solar panel away from the roof and positive when the pressure tends to push the array toward the roof.

The interpretation of the negative results (i.e., pressure and force coefficients) throughout the paper is provided in an absolute sense without regard to their sign.

Results and Discussion

Local mean pressure peak pressure coefficients (surface pressures) and mean and peak force coefficients (net pressures) are presented in the following sections. Their vulnerability with respect to the size of the air clearance underneath the solar array—mainly from aerodynamic perspectives—is discussed.

Mean Pressure Coefficients and Force Coefficients

Investigation of the wind pressure induced on the top and bottom surfaces of the panels shows that the panel surfaces are dominated by negative pressure (suction) for all wind directions. Figs. 6 and 7 provide the maximum negative mean pressure coefficients over the panel bottom and top surface (in an absolute sense) for each wind direction, respectively. Thus, the values provided in these figures are the worst local mean suction induced on the panel surfaces at each particular wind direction. As illustrated, the bottom surface mean suctions within the individual array clearance are generally of higher severity than the corresponding values of the top surface for wind directions from 15° to 45°. Conversely, the opposite trend for a certain clearance height is observed with respect to the distribution of the surface suctions at wind direction between 135° and 165°. The presence of vortices detached from the leading edges of the roof at oblique wind directions has surely played a significant role in influencing the distribution of the surface pressure (Banks 2013; Wang et al. 2020b). The wind suctions induced on the surfaces have further escalated and spread to a larger region over the array's panels mainly due to the separation of the conical vortices, which has a downflow nature at the higher edge of the panels. The interaction among these conical vortices and solar panels yielded localized phenomena, such as wake regions and stagnation points beneath the solar panels at wind directions from 15° to 45° and separation bubbles above the panels at wind directions from 135° to 165°, which are influential in impacting the surface pressures with the wind direction.

In line with the previous study of Wang et al. (2020b), the effect of the array clearance on the bottom surface mean pressure coefficients is more pronounced than those of the top surface. As shown in Fig. 6, the maximum mean pressure coefficients on the bottom surface have greatly decreased in value with decreasing the clearance above the roof, particularly marked at wind directions from 15° to 75° for the front panel A and from 0° to 30° for the other panels of the array. A likely scenario would suggest that disturbance of the wake region formulation on the bottom surface for winds blowing from the front (i.e., 0°–30°) might have accounted for the decrease in the mean suction of the bottom surface with decreasing the size of the array clearance. In this regard, the distribution of the local mean surface pressure and force coefficients will be examined at particular wind directions, including 0°, 45°, 135°, and 180°.

Fig. 8 provides the local distribution of the mean wind pressure coefficients on the bottom and top surface and the mean force coefficients for modules located at the side edge of the array (M1 as named in Fig. 3) for wind directions of 0° and 180°. As shown in Fig. 8(a), placing the array at a smaller clearance ($G = 20$ cm) or directly on the roof ($G = 0$ cm) reduced the positive mean force coefficients (downward net pressures) at 0° wind direction, greatly 10 at regions close to the edges of the modules. This tendency comes as a result of the reduction in the mean pressure coefficients on the bottom surface of the modules installed at clearance height $G = 0$ and $G = 20$ cm.

As shown in Fig. 8(b) for 180°, minimizing the array clearance, either to $G = 0$ or $G = 20$ cm, tends to decrease the negative mean pressure coefficients of the bottom surface, particularly at regions close to the lower edge of the modules of the downstream panels. Regarding the top surface, the negative pressure coefficients of the modules of the downstream panels at no clearance (panels A and B at $G = 0$) have only been affected. Therefore, the decrease in the array clearance to $G = 20$ cm and the concomitant decrease in the bottom surface pressure naturally led to increasing the negative mean force coefficients (higher upward net pressures).

Fig. 9 shows the local distribution of the surface mean pressure and mean force coefficients of modules located at the side of the array (M1) at 45° and 135° wind directions. As clearly shown, the suctions on the top surface seem to have been slightly affected by the air clearance. The mean pressure coefficients of the bottom surface of the upstream panels (A at 45° wind and H at 135° wind) are significantly reduced at no clearance ($G = 0$); see Figs. 9(a and c). 11 As reported by the CFD study of Wang et al. (2020a), these modules are mostly far from the building edge conical vortices. On the other hand, there is an inverse correlation between the clearance height and the bottom surface mean pressure coefficients of the downstream panels (G, F, E, D, C, and B) at 135° wind direction, such that the highest suctions are induced when the array is placed at no clearance ($G = 0$). 12

Consequently, the positive mean force coefficient of modules less interfered by the conical vortices, namely, windward modules of the solar panels A, B, and C at 45° wind direction, are decreased when placing the panels at no clearance, largely at regions close to the lower edge of the panels, as shown in Figs. 9(a and b). Otherwise, the positive mean force coefficients do not necessarily depend on the underneath array clearance. Furthermore, the negative mean force coefficients of the downstream modules (G to A) are greatly decreased at no clearance ($G = 0$), significantly at the regions close to the higher edge of the panels, as shown in Figs. 9(c and d).

The effects of the air clearance on the wind suction induced on the bottom surface of the solar modules are indeed associated with wind interference of the solar panels. Thus, the size of the air

PROOF ONLY

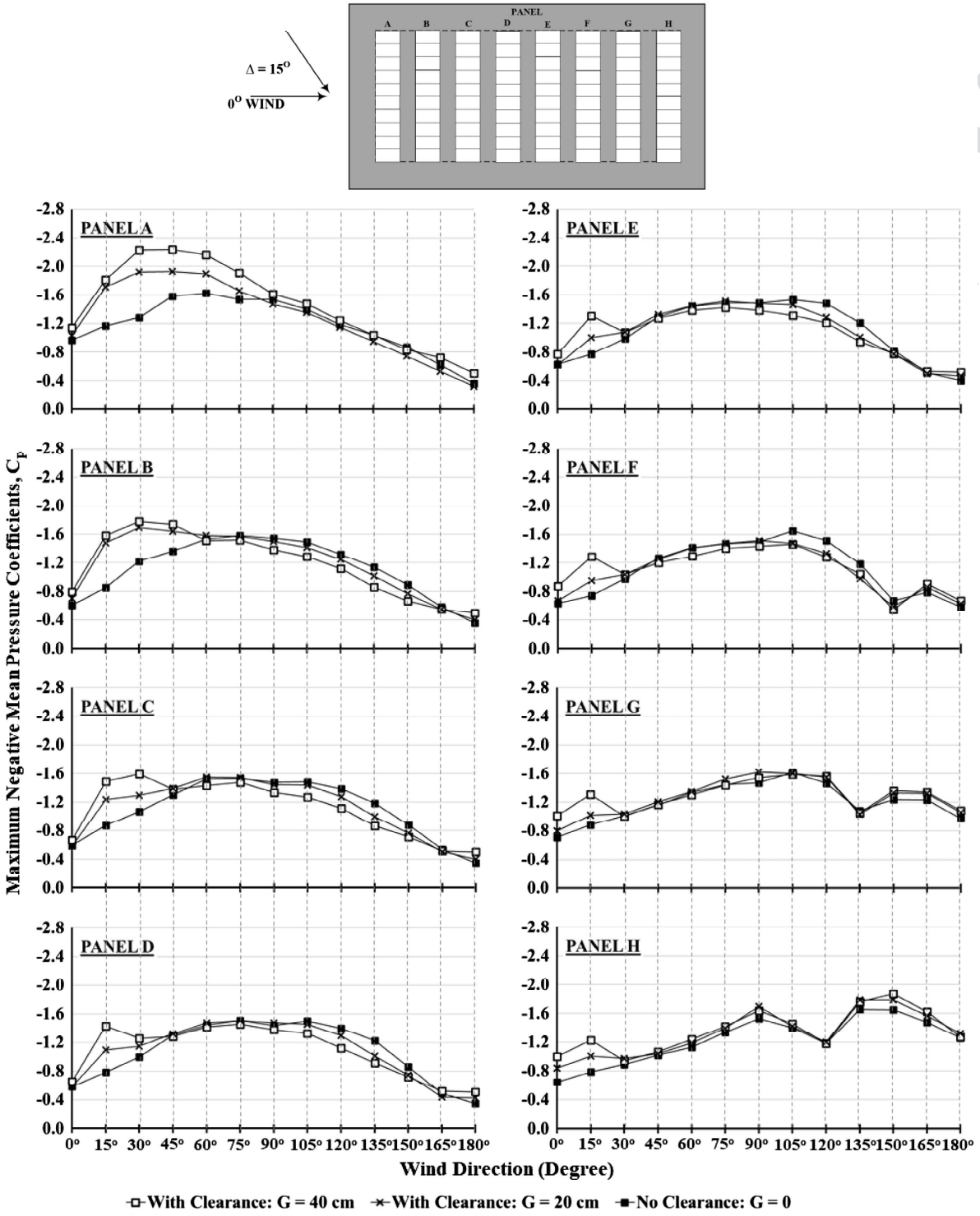

F6:1 **Fig. 6.** Maximum local negative mean pressure coefficients over the panel bottom surface for each wind direction.

clearance affects the impact of the wind interference of the solar panels. As clearly shown from the mean pressure distribution on the bottom surface of all panels at 0° wind and the upstream panels at 45° wind, placing the array at lower clearance would enhance wind interference of the solar panels and disturb the flow separation at the higher edge of the panels. This results in a wake region formulation of a lower vortex frequency.

The same applies to the distribution of the mean pressure coefficients on the bottom surface at winds blowing from behind (i.e., all panels at straight wind and upstream panel for oblique winds such as 180° and 135°, respectively). Placing the array at no clearance would confine the airflow underneath the bottom surface of the panels, and hence this will further disturb the wake region formulation. Regarding the downstream panels at oblique wind direction, the shear layer of the confined wake region is enhanced by the shear layer of the top surface of the upstream panel inducing higher suction on the bottom surface. On the other hand, when there is enough clearance underneath the panels the flow will reattach on

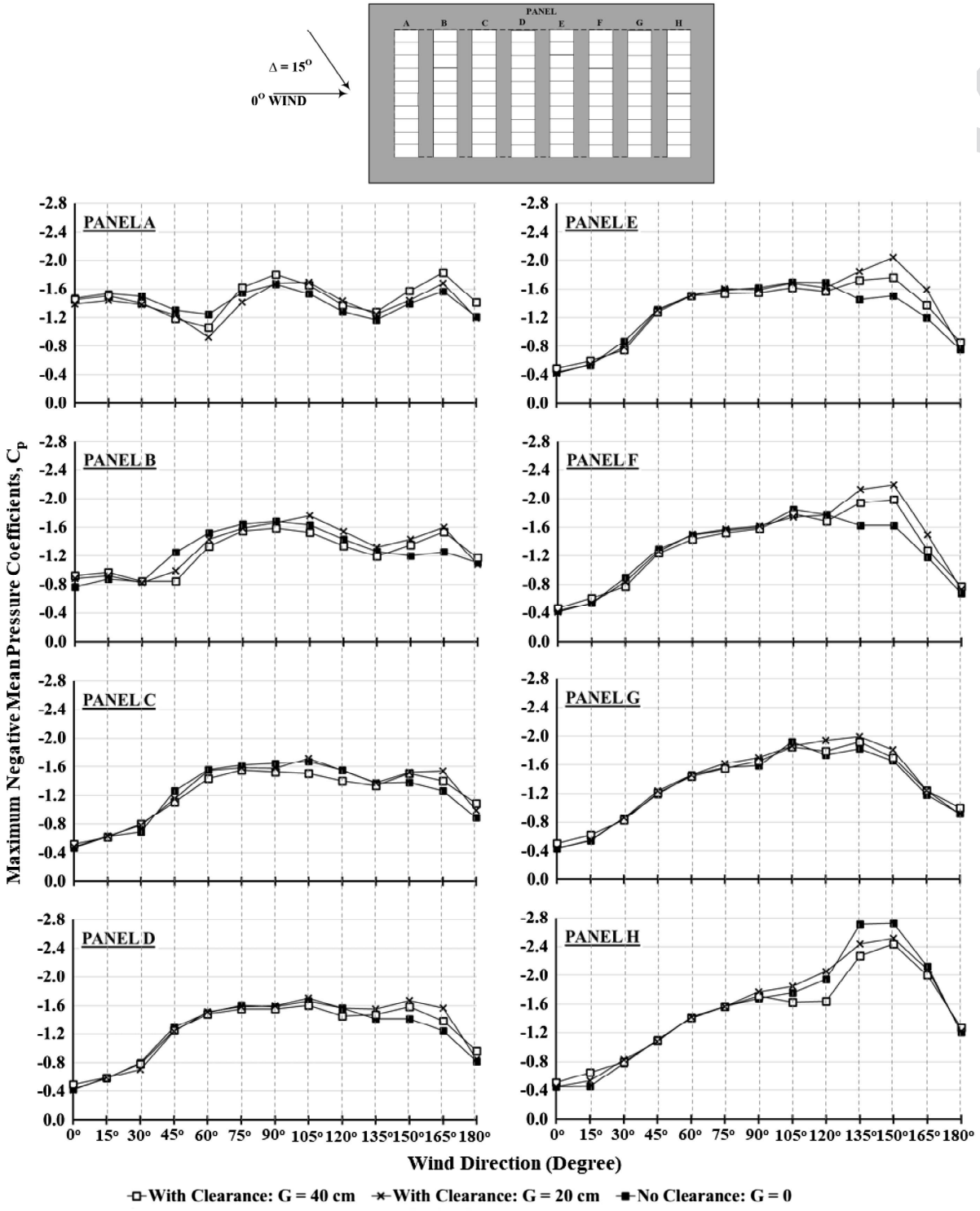

F7:1 **Fig. 7.** Maximum local negative mean pressure coefficients over the panel top surface for each wind direction.

the roof and penetrate with less interference with the wake region on the bottom surface of the upstream panel.

Finally, another point that should be stressed is the highly elevated negative mean force coefficients observed at reducing the array clearance to $G = 20$ cm; see, for instance Figs. 8(b) and 9(c and d). This is indeed a result of the increased suction on the top surface at wind directions from 135° to 180° (Fig. 6), which enhances the net pressure to act upward. Thus, the array at lower clearance would augment the wind interference of the solar panels, causing further attenuation in the wake region on the bottom surface and further intensifying the vortices on the top surface shed from the higher edge of the panels.

Peak Pressure Coefficients and Force Coefficients

Previously, it was demonstrated through the distribution of the mean surface pressure and the mean force coefficients that the solar array clearance above the roof led to altering the conditions of the

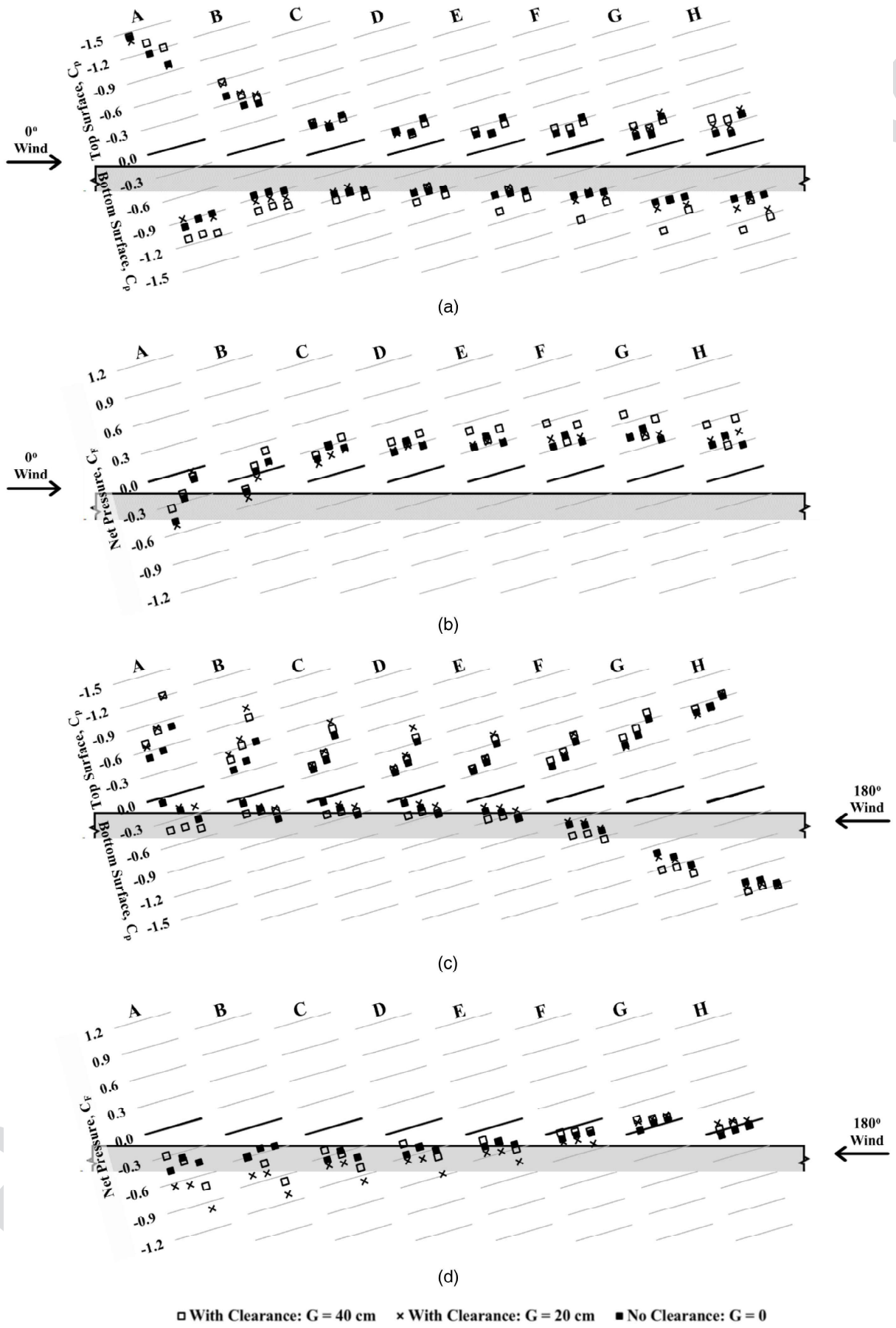

F8:1 **Fig. 8.** Clearance effect on local mean pressure and force coefficients (C_P and C_F) at the edge of the array (module M1) at wind direction (a and b) 0°;
F8:2 and (c and d) 180°.

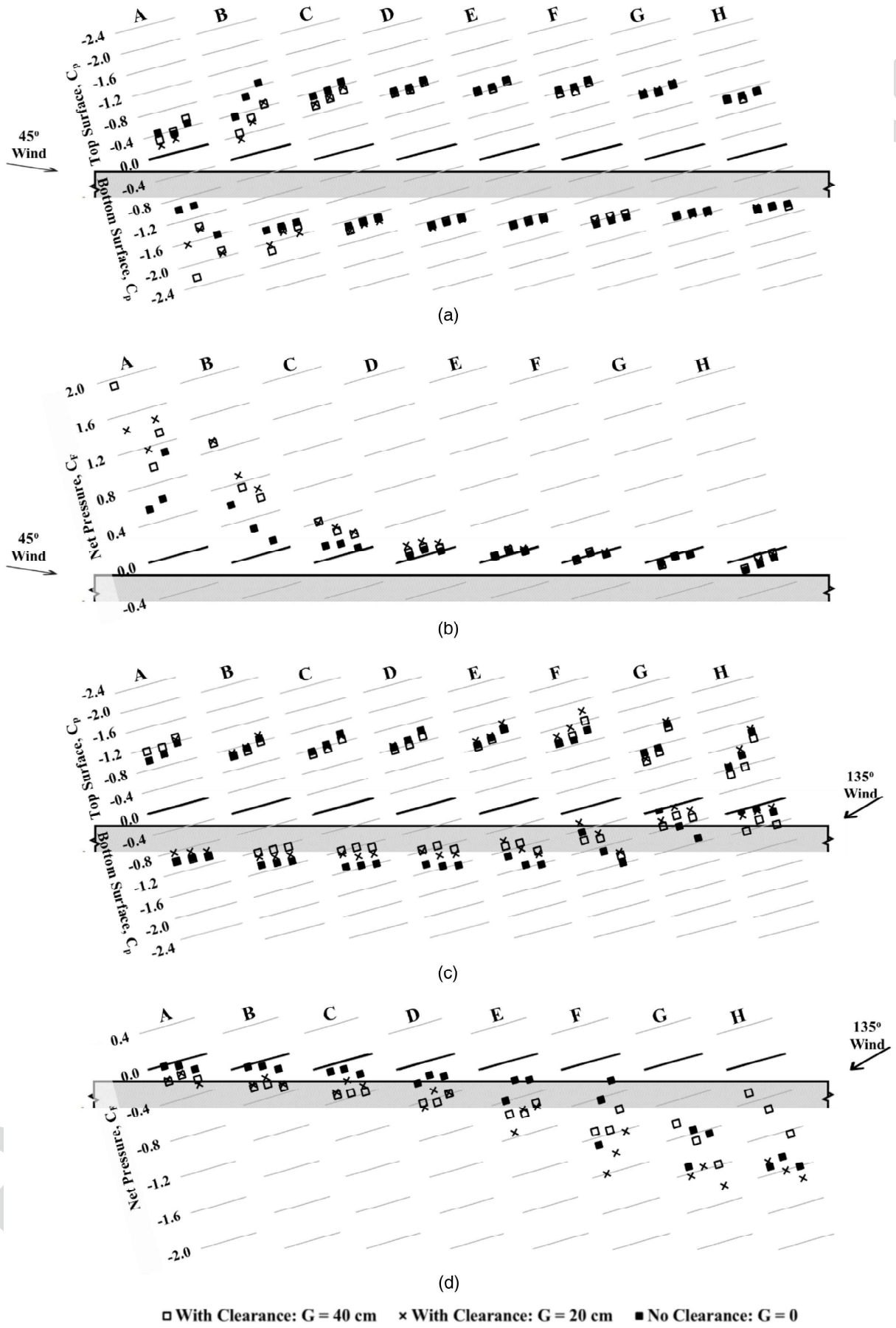

F9:1 **Fig. 9.** Local mean pressure and force coefficients (C_P and C_F) at the windward edge of the array (module M1) at wind direction (a and b) 45°; and
F9:2 (c and d) 135°.

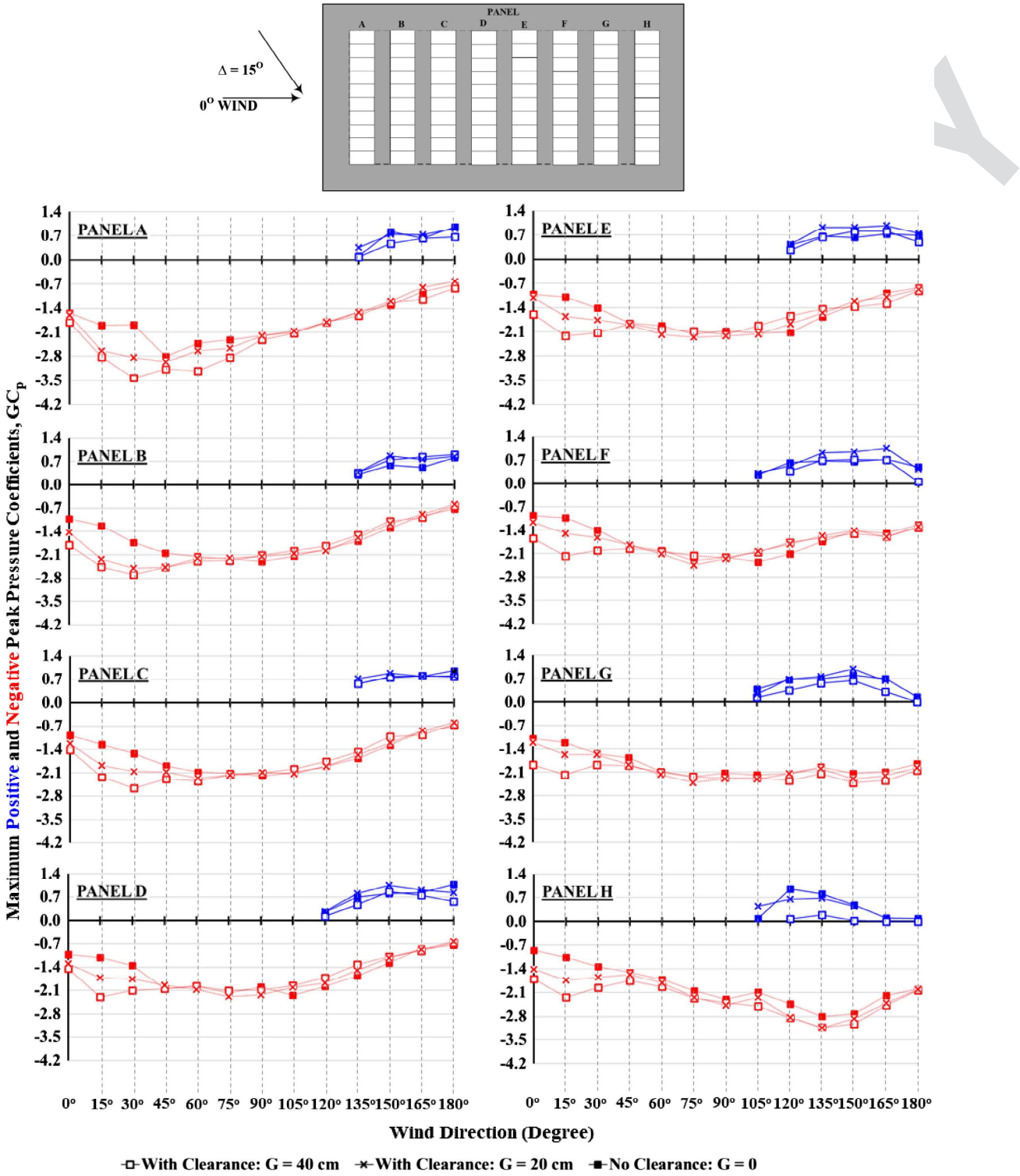

F10:1 **Fig. 10.** Maximum local positive and negative peak pressure coefficients of the panel bottom surface at each wind direction.

flow around panels of the solar array. Therefore, it is important to further assess the impact of underneath array clearance on the peak pressures on the surfaces and across the panels represented by the peak pressure and force coefficients, respectively.

Figs. 10 and 11 show the maximum local positive and negative peak pressure coefficients on the bottom and top surfaces for each wind direction, respectively. As illustrated, however, the surfaces (top and bottom) of the panels have been dominantly exposed to peak suction pressure at different clearance conditions underneath the solar array, and changing the clearance resulted in disturbing their severity. A trend is clearly demonstrated on the bottom surface for the most critical wind directions, including the front panel A at 15°–75° winds, middle panels for 15°–30° winds, and back panels for 0°–30° winds. Conversely, with reference to Fig. 11, the maximum negative pressure coefficients of the top surface are relatively unaffected by the clearance height, except for some panels in the

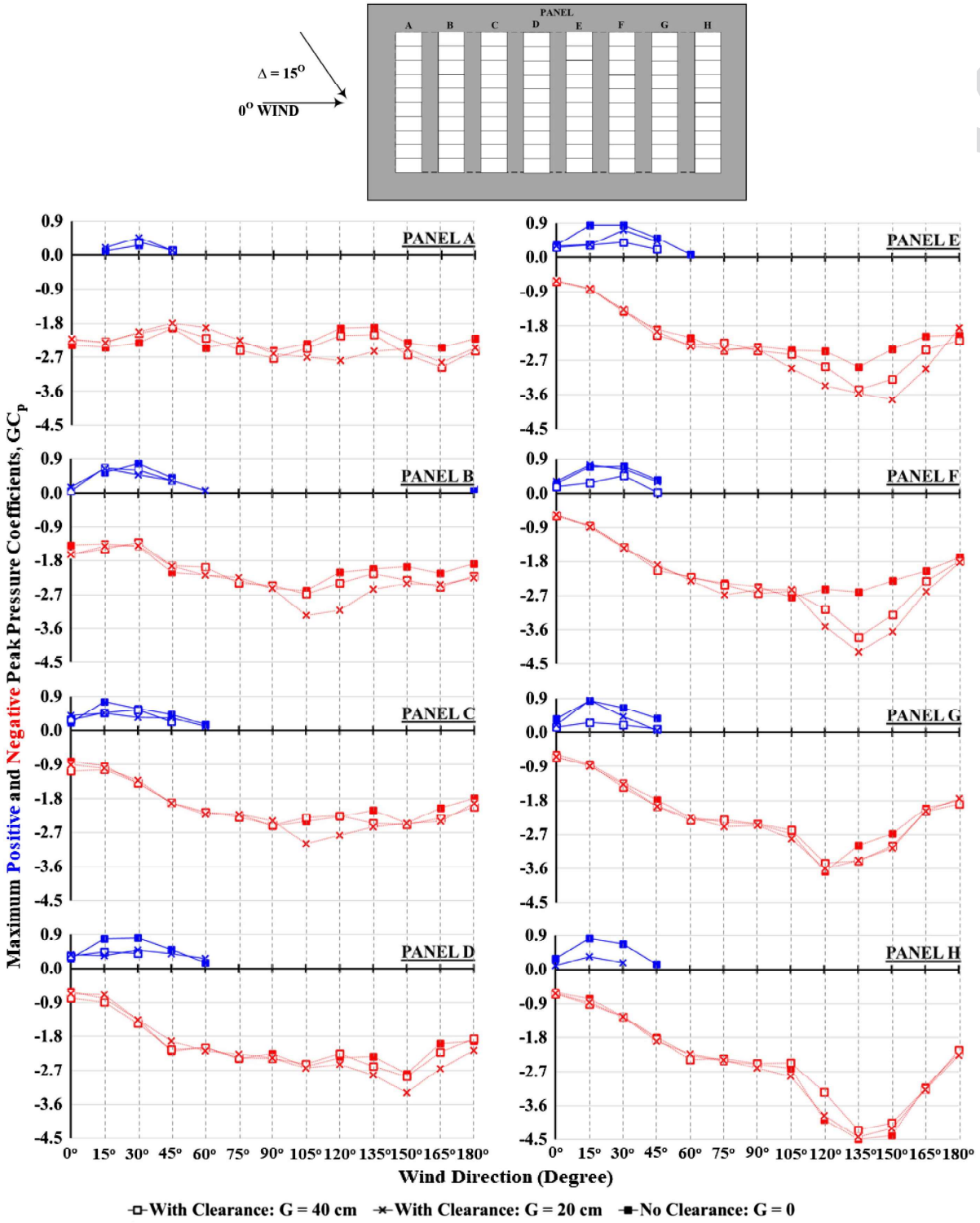

F11:1 **Fig. 11.** Maximum local positive and negative peak pressure coefficients of the panel top surface at each wind direction.

middle of the array (e.g., E and F) at the most critical wind directions ranging from 120° to 165°.

In detail, the negative peak pressure coefficients on the bottom and top surfaces are significantly decreased when the array is placed at no clearance ($G = 0$). Also, the size of the clearance ($G =$ 20 cm and $G = 40$ cm) has two countervailing effects on the surface negative peak pressure coefficients. On one hand, the negative peak pressure coefficients on the bottom surface are increased with increasing the solar array clearance, and on the other hand the negative peak pressure coefficients of the top surface are decreased in magnitude with increasing the solar array clearance, as shown in Figs. 10 and 11, respectively.

The impact of the underneath solar panel array clearance will be examined on the local negative and positive peak force coefficients obtained at wind directions 30° and 150° for modules located on the windward edge of the array (module M1, Fig. 3).

Fig. 12 shows clearly that at the most critical wind direction for positive peak net pressure, i.e., 30°, the values of the positive peak

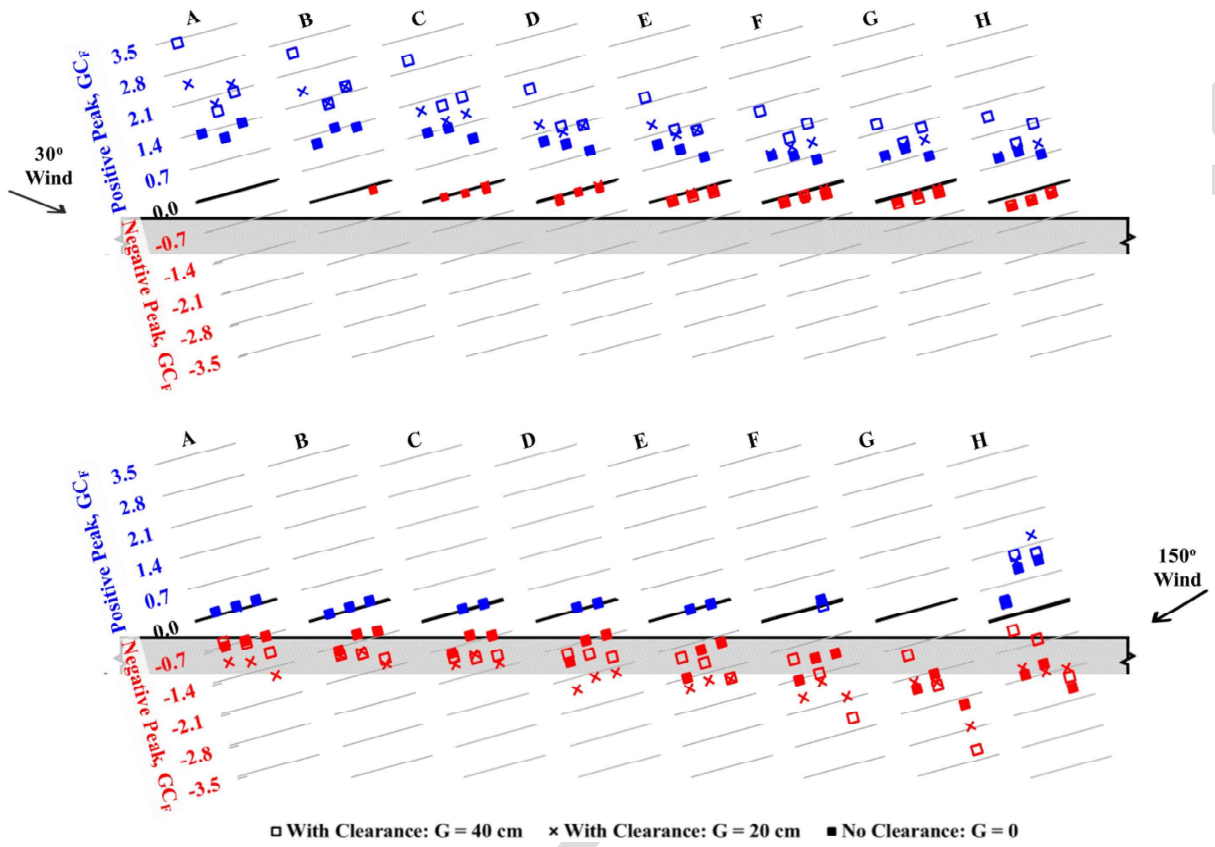

F12:1 **Fig. 12.** Local positive and negative peak force coefficients (GC_F) at the windward edge of the array (module M1) at 30° and 150° wind directions.

force coefficients (GC_F) have decreased, particularly at no clearance ($G = 0$). This is because of the increased bottom surface wind pressure coefficients that played a significant role in equalizing the top surface pressure suction. In contrast, the negative peak force coefficients obtained at the most critical wind direction of 150° are reduced at higher clearance ($G = 40$ cm) at regions close to the lower edge of the panels. The higher values are mostly observed on the modules of lower array clearance ($G = 20$ cm) as the pressure on the top surface becomes greater than the bottom surface reduced pressure.

Impact Assessment in Practice

In this section, the experimental force coefficients that could be treated as design loading are examined and compared in the condition of changing the underneath array clearance. Thus, the experimental force coefficients are calculated in the same manner as the design force coefficients adopted by different national wind codes and standards for roof-mounted solar panels. For instance, the North American wind codes and standards (NRCC 2015; SEAOC 2017; ASCE 2022) adopt the envelope procedure (i.e., the envelope wind tunnel data from all wind directions) for the design force coefficients; while the Japanese industrial standard (Japanese Standards Association 2017) considers the force coefficients for 0° and 180° wind directions.

Figs. 13 and 14 present the maximum mean and maximum peak values of the module force coefficients (worst force coefficient within the panel at a particular wind direction that corresponds to an effective wind area $A = 2.0$ m^2). Following the design value definition of JIS C 8955 (Japanese Standards Association 2017), the module maximum positive mean and peak force coefficients are obtained at 0° wind direction (as presented in Fig. 13), whereas the module maximum negative mean and peak force coefficients are obtained at 180° wind direction (as presented in Fig. 14). It is evident that the clearance of the solar array above the roof has influenced the estimation of the force coefficients intended for design purposes.

The module maximum positive mean and peak force coefficients show a tendency to increasee with increasing the clearance between the solar array and the roof. However, as in Fig. 13, the module maximum positive peak force coefficients of the upstream panel (A) obtained at lower clearance ($G = 20$ cm) are the highest. Thus, the positive mean and peak module force coefficients are increasingly underestimated with the downstream panels at minimizing the clearance of the solar panels (i.e., $G = 0$ and 20 cm). Certainly, that tendency is attributable to the decrease in the local net pressures at regions close to the lower and higher edges of the panel, because most dropped by half compared with the corresponding values of the array placed at higher clearance (i.e., $G =$ 40 cm). The modules of the upstream panel (A) do not experience mean force coefficients except locally at the regions close to the lower edge of the array at $G = 40$ cm where the local mean force coefficient is found to be about 0.2.

As shown in Fig. 14, the module negative force coefficients of the upstream panel (H) are greatly increased when $G = 0$. In the downstream direction, minimizing the clearance from $G = 40$ cm to $G = 20$ cm has generally resulted in overestimating the negative module force coefficients.

Fig. 15 shows the extreme negative and positive peak force coefficients, which are assessed as loading force coefficients by the National Building Code of Canada (NRCC 2015), SEAOC PV2 (SEAOC 2017), and ASCE/SEI 7 (ASCE 2022), among the

PROOF

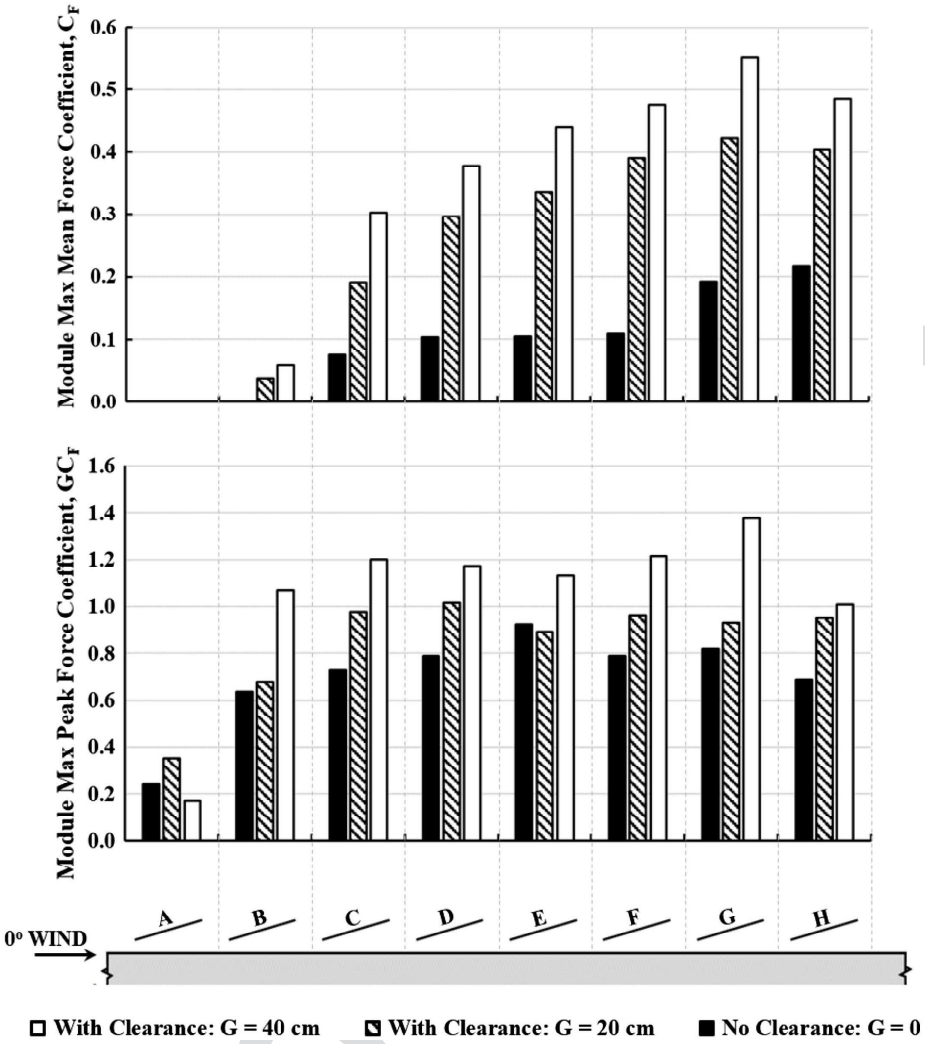

F13:1 **Fig. 13.** Effect of clearance on module maximum positive mean and peak force coefficients at 0° wind direction.

considered air clearances versus the effective wind area of the panel. The extreme force coefficient corresponding to a particular effective area is the envelope value from all wind directions and all possible loading areas within the panel. Overall, these results are in accordance with findings reported by Kopp (2014) wherein the worst extreme peak force coefficients (i.e., the envelope of the envelope panels' curves) would show little difference with the underneath array clearance. This fact is acknowledged, but there is a considerable discussion to take place in this regard. The study of Kopp (2014) lacked the potential to quantify the clearance effect because of some technical limitations of the experimental modeling. In the experimental modeling of that study, the pressure taps coverage on the bottom surface of the panels is reduced compared with the top surface, where three lines of pressure taps were considered as opposed to only one line along the center of the bottom surface. Excluding the pressure taps on the bottom surface at regions close to the edges led to the conclusion that the array clearance has a minimum impact on the pressure envelope curves, although such regions are highly affected by the clearance at critical wind directions, as demonstrated subsequently in the present study and that of Wang et al (2020b).

Referring to the extreme peak force coefficient of Fig. 15, placing the solar array at different clearances above the roof had uneven extreme peak force coefficients. The topology of the differences between the measurements among the considered clearances can be summarized as follows: Differences resulting in the extreme negative peak force coefficients by placing the array at half or zero of the typical clearance vary spatially depending on the panel location within the array. Differences resulting in the extreme positive peak force coefficients by placing the array at half of the typical clearance show a strong correlation with the effective wind area of the panel and less correlation with the panel location. Differences resulting in the extreme positive peak force coefficients by placing the array at zero of the typical clearance show a correlation with the effective wind area of the panel and the panel location within the array.

In detail, the results provided in Fig. 15 demonstrate that placing the solar array at no clearance ($G = 0$) largely diminishes the extreme positive peak force coefficients of most of the array panels, particularly the values of the front panels (A and B) and those corresponding to the area of one module or less (GC_F of $A \leq 2.0$ m^2) of the middle and the back panels. Clearly, the extreme positive peak force coefficients of the front panels at no clearance ($G = 0$) are reduced by one-third. Although the extreme negative peak force coefficients are found to be less affected with placing the array at no clearance ($G = 0$), an increasing tendency is observed on the extreme negative force coefficients of the back panels (G and H) with a factor up to 1.6. In general, minimizing

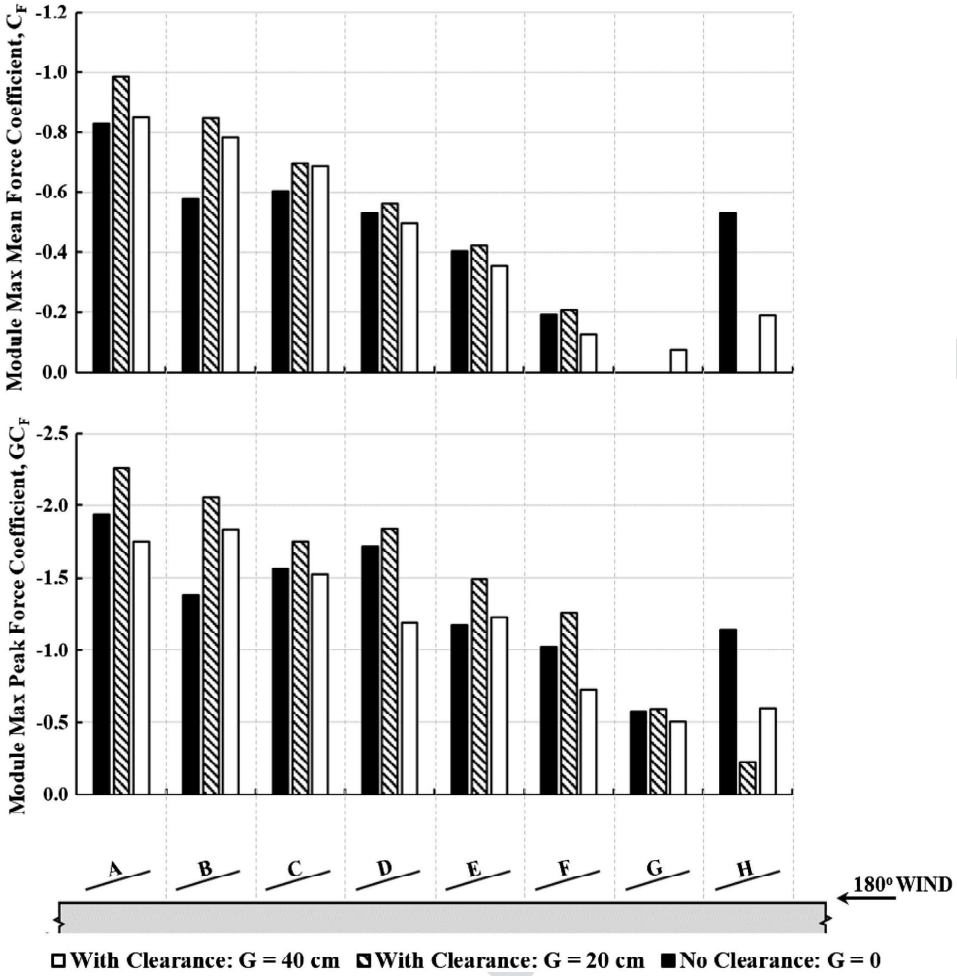

F14:1 **Fig. 14.** Effect of clearance on module maximum negative mean and peak force coefficients at 180° wind direction.

the underneath array clearance (i.e., from $G = 40$ cm to $G = 20$ cm) tends to decrease the extreme positive peak force coefficients and to largely increase the extreme negative peak force coefficients.

As stated previously, the current wind codes and standards do not incorporate the impact of the underneath clearance of the solar array above the roof. Specifically, the provisions adopted by the National Building Code of Canada (NRCC 2015), SEAOC PV2 (SEAOC 2017), and ASCE/SEI 7 (ASCE 2022) are applicable exclusively for solar panels installed at a clearance height of 60 cm or less ($G \leq 60$ cm) based on the premise that the air clearance has no bearing within that limit. However, the results of the present study confirm that the underneath air clearance of the solar array presents different tendencies for the extreme force coefficients according to the direction of the net pressure (upward or downward).

To give a clearer illustration of the potential distortions that could be introduced on the design loading coefficients, Fig. 16 shows the experimental module and panel extreme (envelope) lift and drag force coefficients, which are practically used to design the supports of the solar panel racking systems. Thus, the upward lift forces and the drag forces are respectively used to evaluate the vertical and the horizontal resistance of the posts (in case of mechanically fastened racking systems on roofs) or weights (in case of roof ballasted racking systems).

As clearly illustrated in Fig. 16, minimizing the underneath solar array clearance would require increasing the upward resistance of the racking system because the upward lift forces of the modules and the panels broadly increased by 50% when the typical underneath clearance was reduced to half. It is true that the negative lift force coefficients show a reversed trend, but these forces act as a downward thrust on the roof. Thus, increasing the clearance is detrimental to the vertical wind loads transferred to the roof.

Changing the underneath clearance size also influences the drag coefficients. In this case, the comparison shall be made without considering the direction of the drag forces (left or right) because they are perceived as horizontal resistance required by the supports of the racking system. Accordingly, comparing the worst values of the positive and negative (right and left, respectively) extreme drag force coefficients shows that reducing the clearance to half resulted in enlarging the drag coefficients of the middle panels by 30% and the back panel by 60%. To a lesser extent, placing the array at no clearance reduced the drag resistance of the module and the entire panel by 20% of the upstream panels (A, B, C, and D) and on the other side enlarged the drag coefficients of the back panels by 30%.

The results provided in this section revealed that the wind tunnel experimental results assigned as design force coefficients are particularly sensitive to air clearance underneath the solar array model; therefore, such coefficients based on violating such geometry layout may compromise the credibility of the design and the safety of the structures, particularly when the results imply underestimation. The provided results may also assist solar panel practitioners and

PROOF COPY

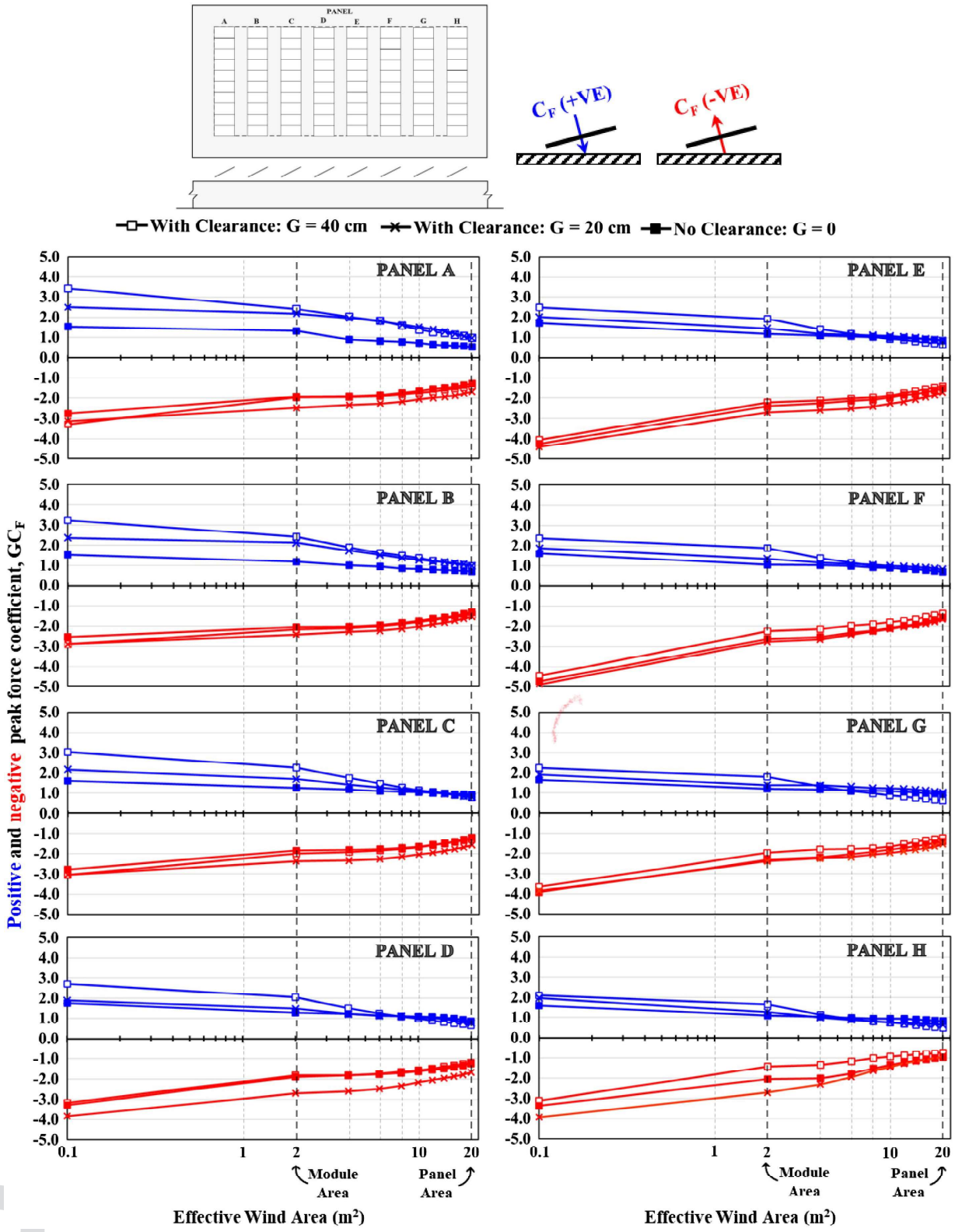

F15:1 **Fig. 15.** Effect of clearance on extreme positive and negative area-averaged peak force coefficients, envelope GC_F.

engineers in this concern, which is not specifically dealt with in existing codes and standards provisions. Finally, it is important to sensitize the code and standards community to research issues that may be critical to be addressed in the codification process considering, of course, the inherent error associated with such measurement procedures.

Summary and Conclusions

In the present experimental investigation, the impact of the air clearance between the solar array and the roof surface was examined by considering a solar array of eight panels mounted on a building with a flat roof at three air clearance heights above the

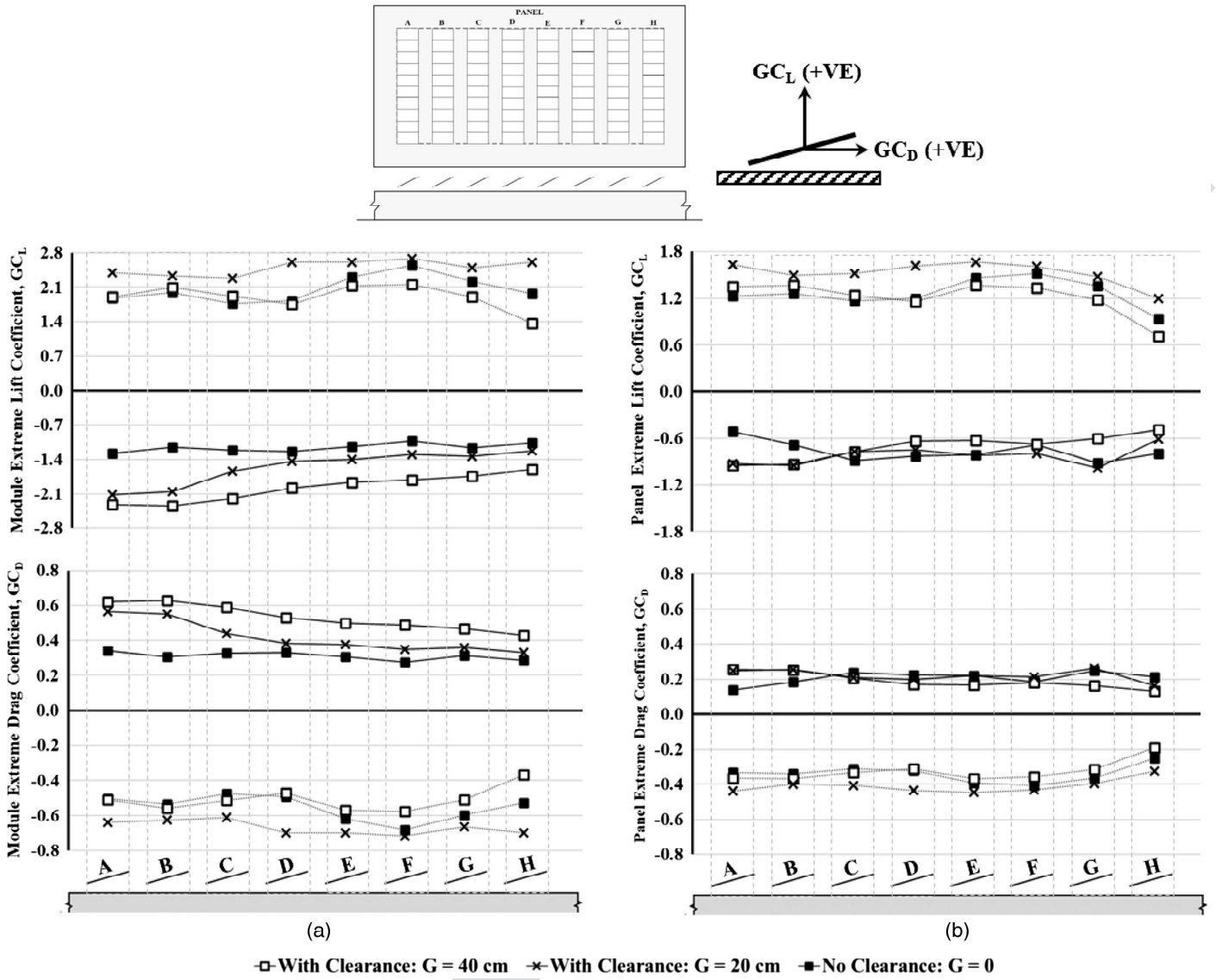

F16:1 **Fig. 16.** Extreme peak lift and drag force coefficients (GC_L and GC_D) for (a) solar module; and (b) solar panel.

roof, namely, 40.0 cm (typical), 20.0 cm (reduced), and 0 cm (no clearance).

In effect, this paper thoroughly discussed the aerodynamic and the design aspects of varying the air clearance underneath the array, and thus the following key conclusions can be drawn:

- Varying the air clearance size may twist the flow-array interaction out of shape and may affect the local phenomena responsible for producing high suctions on the bottom surface, particularly like the wind interference of the solar panels. The wake region formulation is disturbed depending on the panel location and wind direction.
- Varying the air clearance has implications on the mean and peak values of the surface and net pressures. Wind-induced pressure on the bottom surface has been found to be the most sensitive to varying the air clearance for winds from 0° and 30°. Generally, the nearer the array is to the roof, the greater the upward net pressures and the lower the downward net pressures.
- Condoning the air clearance during the experimental modeling setup is not appropriate practice, and hence modeling of this layout feature at minimal blockage is indeed important.
- There is a risk that in the event of snow accumulation around the solar panels, the wind may become more severe on the back and middle panels. For regions exposed to snow frequently, it is recommended to consider the excess of the wind-induced pressure at these panels of the array.

Finally, the present study provides a comprehensive response for the array clearance implications on wind loading of solar panels tilted on flat roofs. The research outputs could be adopted by rooftop solar panel professionals to rectify the design values given that the effects of air clearance are addressed unsatisfactorily by the current provisions of wind codes and standards.

Data Availability Statement

Some or all data, models, or code that support the findings of this study are available from the corresponding author upon reasonable request.

Acknowledgments

The authors are grateful for the financial support from the Natural Sciences and Engineering Research Council of Canada (NSERC) for the present research.

References

Alberta Infrastructure. 2017. *Solar photovoltaic guidelines: Planning and installation for Alberta infrastructure projects*.

Alrawashdeh, H., and T. Stathopoulos. 2015. "Wind pressures on large roofs of low buildings and wind codes and standards." *J. Wind Eng. Ind. Aerodyn.* 147 (Dec): 212–225. https://doi.org/10.1016/j.jweia.2015.09.014.

Alrawashdeh, H., and T. Stathopoulos. 2020. "Wind loads on solar panels mounted on flat roofs: Effect of geometric scale." *J. Wind Eng. Ind. Aerodyn.* 206 (Nov): 104339. https://doi.org/10.1016/j.jweia.2020.104339.

Aly, A. M. 2016. "On the evaluation of wind loads on solar panels: The scale issue." *Sol. Energy* 135 (Oct): 423–434. https://doi.org/10.1016/j.solener.2016.06.018.

Aly, A. M., and G. Bitsuamlak. 2013. "Aerodynamics of ground-mounted solar panels: Test model scale effects." *J. Wind Eng. Ind. Aerodyn.* 123 (Dec): 250–260. https://doi.org/10.1016/j.jweia.2013.07.007.

ASCE. 2021. *Wind tunnel testing for buildings and other structures*. ASCE/SEI 49. Reston, VA: ASCE.

ASCE. 2022. *Minimum design loads and associated criteria for buildings and other structures*. ASCE/SEI 7. Reston, VA: ASCE.

Banks, D. 2013. "The role of corner vortices in dictating peak wind loads on tilted flat solar panels mounted on large, flat roofs." *J. Wind Eng. Ind. Aerodyn.* 123 (Dec): 192–201. https://doi.org/10.1016/j.jweia.2013.08.015.

Candelario, J. D., T. Stathopoulos, and I. Zisis. 2014. "Wind loading on attached canopies: Codification study." *J. Struct. Eng.* 140 (5): 4014007. https://doi.org/10.1061/(ASCE)ST.1943-541X.0001007.

Cao, J., A. Yoshida, P. K. Saha, and Y. Tamura. 2013. "Wind loading characteristics of solar arrays mounted on flat roofs." *J. Wind Eng. Ind. Aerodyn.* 123 (Dec): 214–225. https://doi.org/10.1016/j.jweia.2013.08.014.

Cook, N. J. 1978. "Determination of the model scale factor in wind-tunnel simulations of the adiabatic atmospheric boundary layer." *J. Wind Eng. Ind. Aerodyn.* 2 (4): 311–321. https://doi.org/10.1016/0167-6105(78)90016-8.

Davenport, A. G. 1961. "The spectrum of horizontal gustiness near the ground in high winds." *Q. J. R. Meteorol. Soc.* 87 (372): 194–211. https://doi.org/10.1002/qj.49708737208.

Durst, C. S. 1960. "The statistical variation of wind with distance." *Q. J. R. Meteorol. Soc.* 86 (370): 543–549. https://doi.org/10.1002/qj.49708637012.

Geurts, C., and P. Blackmore. 2013. "Wind loads on stand-off photovoltaic systems on pitched roofs." *J. Wind Eng. Ind. Aerodyn.* 123 (Dec): 239–249. https://doi.org/10.1016/j.jweia.2013.08.016.

Ginger, J., M. Payne, G. Stark, B. Sumant, and C. Leitch. 2011. *Investigations on wind loads applied to solar panels mounted on roofs*. Townsville, Australia: James Cook Univ.

Japanese Standards Association. 2017. *Load design guide on structures for photovoltaic array.* JIS C 8955. Tokyo: Japanese Standards Association.

Kopp, G. A. 2014. "Wind loads on low-profile, tilted, solar arrays placed on large, flat, low-rise building roofs." *J. Struct. Eng.* 140 (2): 04013057. https://doi.org/10.1061/(ASCE)ST.1943-541X.0000825.

Kopp, G. A., S. Farquhar, and M. J. Morrison. 2012. "Aerodynamic mechanisms for wind loads on tilted, roof-mounted, solar arrays." *J. Wind Eng. Ind. Aerodyn.* 111 (Dec): 40–52. https://doi.org/10.1016/j.jweia.2012.08.004.

Leitch, C. J., J. D. Ginger, and J. D. Holmes. 2016. "Wind loads on solar panels mounted parallel to pitched roofs, and acting on the underlying roof." *Int. J.* 22 (3): 307–328. https://doi.org/10.12989/was.2016.22.3.307.

Naeiji, A., F. Raji, and I. Zisis. 2017. "Wind loads on residential scale rooftop photovoltaic panels." *J. Wind Eng. Ind. Aerodyn.* 168 (6): 228–246. https://doi.org/10.1016/j.jweia.2017.06.006.

NRCC (National Research Council Canada). 2015. *National building code of Canada*. Ottawa: NRCC.

Saathoff, P. J., and T. Stathopoulos. 1992. "Wind loads on buildings with sawtooth roofs." *J. Struct. Eng.* 118 (2): 429–446. https://doi.org/10.1061/(ASCE)0733-9445(1992)118:2(429).

SEAOC (Structural Engineers Association of California). 2017. *Wind design for solar arrays*. SEAOC PV2. Sacramento, CA: SEAOC.

Stathopoulos, T. 1984. "Design and fabrication of a wind tunnel for building aerodynamics." *J. Wind Eng. Ind. Aerodyn.* 16 (84): 361–376. https://doi.org/10.1016/0167-6105(84)90018-7.

Stathopoulos, T., and M. Dumitrescu-Brulotte. 1989. "Design recommendations for wind loading on buildings of intermediate height." *Can. J. Civ. Eng.* 16 (9): 910–916. https://doi.org/10.1139/l89-134.

Stathopoulos, T., M. Elsharawy, and K. Galal. 2013. "Wind load combinations including torsion for rectangular medium-rise building." *Int. J. High-Rise Build.* 2 (3): 1–11.

Stathopoulos, T., and A. R. Mohammadian. 1991. "Modelling of wind pressures on monoslope roofs." *Eng. Struct.* 13 (91): 281–292. https://doi.org/10.1016/0141-0296(91)90039-F.

Stathopoulos, T., K. Wang, and H. Wu. 2000. "Proposed new Canadian wind provisions for the design of gable roofs." *Can. J. Civ. Eng.* 27 (5): 1059–1072. https://doi.org/10.1139/l00-023.

Stathopoulos, T., I. Zisis, and E. Xypnitou. 2014. "Local and overall wind pressure and force coefficients for solar panels." *J. Wind Eng. Ind. Aerodyn.* 125 (Feb): 195–206. https://doi.org/10.1016/j.jweia.2013.12.007.

Stenabaugh, S. E., Y. Iida, G. A. Kopp, and P. Karava. 2015. "Wind loads on photovoltaic arrays mounted parallel to sloped roofs on low-rise buildings." *J. Wind Eng. Ind. Aerodyn.* 139 (Apr): 16–26. https://doi.org/10.1016/j.jweia.2015.01.007.

Stenabaugh, S. E., P. Karava, and G. A. Kopp. 2010. *Design wind loads for photovoltaic systems on sloped roofs of residential buildings*.

von Kármán, T. 1948. "Progress in the statistical theory of turbulence." *Proc. Nat. Acad. Sci.* 34 (11): 530–539. https://doi.org/10.1073/pnas.34.11.530.

Wang, J., P. van Phuc, Q. Yang, and Y. Tamura. 2020a. "LES study of wind pressure and flow characteristics of flat-roof-mounted solar arrays." *J. Wind Eng. Ind. Aerodyn.* 198 (Mar): 104096. https://doi.org/10.1016/j.jweia.2020.104096.

Wang, J., Q. Yang, and Y. Tamura. 2018. "Effects of building parameters on wind loads on flat-roof-mounted solar arrays." *J. Wind Eng. Ind. Aerodyn.* 174 (Mar): 210–224. https://doi.org/10.1016/j.jweia.2017.12.023.

Wang, J., Q. Yang, P. van Phuc, and Y. Tamura. 2020b. "Characteristics of conical vortices and their effects on wind pressures on flat-roof-mounted solar arrays by LES." *J. Wind Eng. Ind. Aerodyn.* 200 (May): 104146. https://doi.org/10.1016/j.jweia.2020.104146.

PROOF ONLY